Colloids and Surfaces A: Physicochem. Eng. Aspects 357 (2010) 53–60

Contents lists available at ScienceDirect

Colloids and Surfaces A: Physicochemical and Engineering Aspects

journal homepage: www.elsevier.com/locate/colsurfa

Molecular simulation of collection of methane isotherms in carbon material using all-atom and united atom models

Sebastião M.P. Lucena[a,*], Luis F.A. Frutuoso[a], Pedro F.G. Silvino[a], Diana C.S. Azevedo[a], J.P. Toso[b], G. Zgrablich[b], Célio L. Cavalcante Jr.[a]

[a] Universidade Federal do Ceará, Dept. Eng. Química, Grupo de Pesquisa em Separações por Adsorção – GPSA, Campus do Pici, Bl. 709, 60455-760 Fortaleza, CE, Brazil
[b] Universidade Nacional de San Luis, Laboratorio de Ciencias de Superficies y Medios Porosos, Ejército de los Andes 950, 5700 San Luis, Argentina

ARTICLE INFO

Article history:
Received 2 July 2009
Received in revised form 3 December 2009
Accepted 7 December 2009
Available online 14 December 2009

Keywords:
Methane adsorption
All-atom model
Activated carbon
Pore size distribution
Monte Carlo simulations

ABSTRACT

In this study the performances of all-atom (AA) and united atom (UA) models (fitted and unfitted) of the methane molecule are evaluated for the description of adsorption isotherms on graphite surfaces and in a collection of graphitic slit pores. We simulated collections of isotherms using the grand canonical Monte Carlo method with an all-atom model and adjusted united atom models in graphene layers made up of discrete atoms of carbon. The collections of isotherms are used to determine the pore size distribution (PSD) of four activated carbon samples. We also investigated the sensitivity of the system to the cutoff and solid–fluid standard parameterization. It was found that the simulated AA model isotherm shape on the graphite surface is much more similar to the experimental data than the UA model isotherm. The cutoff had little influence on isotherm and different solid–fluid standard parameterizations change the PSD. We also found that despite presenting similar fitting with the experimental isotherms, the models presented distinct PSDs. The unfitted united atom model (UA1) suggested less plausible PSDs, while the all-atom (AA) and the fitted united atom model (UA2) model provided apparently more realistic estimates of the internal structure of microporous carbons.

1. Introduction

Activated carbon materials have been studied for systems of energy storage based on natural gas. One of the difficulties to obtain activated carbon materials of high storage capacity is related to an accurate determination of the pore size distribution (PSD) of the real activated carbon due to the non-structured nature of these materials.

The generation of a database of local isotherms based on Monte Carlo or NLDFT methods with predictive capability and consistency has become a standard procedure to obtain PSDs [1–3]. The use of methane as the probe-gas for this type of characterization has the advantage of testing the activated carbon in the same conditions of the specific application (NG storage, for example). However, some studies indicated discrepancies between PSDs obtained using methane and other probe-gases [4–6]. The reason for discrepancies may be related to the simplified models (activated carbon and methane) and the specific parameters for intermolecular interactions.

This study has two main objectives. First, we shall investigate how the atomic model of the methane molecule can influence the PSD. Although methane all-atom (AA) models are known to yield better liquid and solid behavior of homogeneous fluid than united atom (UA) models [7–10] and a general availability of AA models in literature, their use in adsorption has been rarely investigated. This may be explained by the longer computational times of AA models. So we would like to evaluate if UA models are as good as AA models. Also, we would like to know the importance of validated parameters of intermolecular interactions in supercritical conditions. For fluid–fluid systems, these parameters usually present a good description of the bulk liquid–gas equilibrium data or bulk liquid properties [5,7]. For solid–fluid systems, the standard parameterization is to reproduce reference experimental adsorption isotherms on nonporous graphite [11]. In the present study, we are interested on the impact of the solid–fluid parameterization. We selected two methane united atom models, fitted and unfitted to nonporous graphite surface, to evaluate their performance in describing real activated carbons PSDs.

2. Model development (theory)

2.1. Methane and carbon models

We chose the AA model proposed by Murad and Gubbins [8], normally used in molecular dynamic simulation studies. Recently, Stassen [10] made comparisons between 13 different methane

* Corresponding author. Tel.: +55 85 32442296.
E-mail address: lucena@ufc.br (S.M.P. Lucena).

0927-7757/$ – see front matter © 2009 Elsevier B.V. All rights reserved.
doi:10.1016/j.colsurfa.2009.12.015

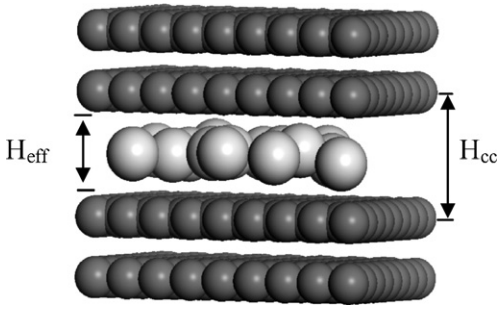

Fig. 1. Model of the slit pore used with main dimensional parameters. H_{eff}: effective internal pore size; H_{cc}: carbon center-to-center pore size.

models and concluded that the Murad and Gubbins potential produces more realistic properties for liquid methane.

The first selected UA model was a modified Sweatman and Quirke model [5] that was named UA1. All comparisons with the AA model were done with this model. We slightly altered the solid–solid parameter of the original Sweatman and Quirke UA model so that it matched the CH_4 simulated isotherm of the AA model in a graphene surface (see details in Section 3.1). By doing this we shall be able to compare the impact of the AA and UA models on the PSDs.

Starting from the same model of Sweatman and Quirke, a second adjustment was made so that the simulated isotherm matched the CH_4 experimental isotherm on Vulcan, a reference graphite surface. This new model was named UA2.

The carbon was modeled with a slit-shaped simulation cell of 40 Å × 40 Å with walls made of two layers of graphene sheets. The graphene sheets are made up of discrete atoms of carbon. We did not use the graphitic Steele potential surface as current in the carbon literature. The simulation cell with the main parameters is shown in Fig. 1. For conditions in which low densities were expected, the unit cells were connected side-by-side to increase the simulation cell volume and enhance the number of molecules in the simulation.

2.2. Intermolecular interactions

The fluid–fluid interaction was calculated from the classical 12–6 LJ (Lennard–Jones) potential equation:

$$U(r_{ij}) = 4\varepsilon_{ij}\left[\left(\frac{\sigma_{ij}}{r_{ij}}\right)^{12} - \left(\frac{\sigma_{ij}}{r_{ij}}\right)^{6}\right]$$

where ε_{ij} is the well depth, σ_{ij} is the diameter, and r_{ij} is the distance between interacting atoms i and j. All parameters can be seen in Table 1.

Since we use graphene layers made up of discrete atoms of carbon instead of single graphitic Steele potential surface for representing the graphene layers, all the interactions between solid and fluid were also described by LJ potentials (see Table 1). The cross terms were obtained using arithmetic and geometric combination rules. Graphene layers made up of discrete atoms are very CPU time demanding but may better represent the corrugation of the surface and are also more appropriate to the subsequent development of more sophisticated structural models of porous carbons as, for example, in the case of reverse Monte Carlo techniques [13].

Table 2
Simulated values for minimum adsorption slit and excludes pore width.

Model	Minimum adsorption slit, $H_{cc\,minimum}$ (Å)	Excluded pore width, H_e (Å)
AA	6.6	2.78
UA1	6.4	2.7
UA2	6.4	2.7

2.3. Simulation details

Grand canonical Monte Carlo (GCMC) technique was used in the simulation of adsorption isotherms. The algorithm allows displacements (translations and rotations), creations, and destructions. These simulations consisted of evaluating the average number of adsorbate molecules for which the chemical potential equals that of the bulk phase at a given pressure and temperature. Details of the method can be seen elsewhere [14]. The output of such a simulation is the absolute adsorbed amount, whereas experimentally the excess adsorbed amount is the property that is measured. The excess amount was calculated by subtracting the simulated absolute amount from the total number of molecules present in the pore effective volume calculated with the Peng–Robinson equation of state. Details of the procedure can be seen in Refs. [3,15].

The GCMC simulations were performed on a PC Dell workstation (Intel dual core, 3.0 GHz processor), using the Material Studio Sorption code [16]. Prior to the production phase, 1.5×10^6 equilibration steps were carried out. Between 2 and 3×10^6 production steps were performed in order to calculate mean values. To check the production phase convergence we have tested representative pores for 1, 2 and n methane layers up to 7×10^6 Monte Carlo steps, without significant change in the results. The potential cutoff distance was 14 Å, with a low cutoff (bad contact rejection distance) of 0.4 Å.

2.4. Local isotherm databases

Local isotherm databases were simulated in 24 pores ranging from a maximum distance between the centers of carbon atoms H_{cc} = 53 Å and a minimum H_{cc} that was defined empirically by molecular simulation [3]. Monte Carlo simulation was done until the smallest pore in which adsorption of various methane models molecules was possible. The minimum adsorption slit ($H_{cc\,minimum}$) for each model is shown in Table 2. The values are within the order of magnitude found by Gusev et al. [3], which was 6.3 Å for an UA

Table 1
LJ potential parameters for fluid–fluid and solid–fluid interaction.

	σ_{ff} (Å)	ε_{ff} (kcal mol^{-1})	σ_{ss} (Å)	ε_{ss} (kcal mol^{-1})
UA1 model	3.7[a]	0.295[a]	3.4[b]	0.044[c]
UA2 model	3.7[a]	0.295[a]	3.4[b]	0.049[c]

	$\sigma_{ff\,C-C}$ (Å)	$\sigma_{ff\,H-H}$ (Å)	$\varepsilon_{ff\,C-C}$ (kcal mol^{-1})	$\varepsilon_{ff\,H-H}$ (kcal mol^{-1})	σ_{ss} (Å)	ε_{ss} (kcal mol^{-1})
AA model	3.35[d]	2.813[d]	0.1017[d]	0.0171[d]	3.4[b]	0.055[b]

[a] Sweatman and Quirke [5].
[b] Steele [12].
[c] This work.
[d] Murad and Gubbins [8].

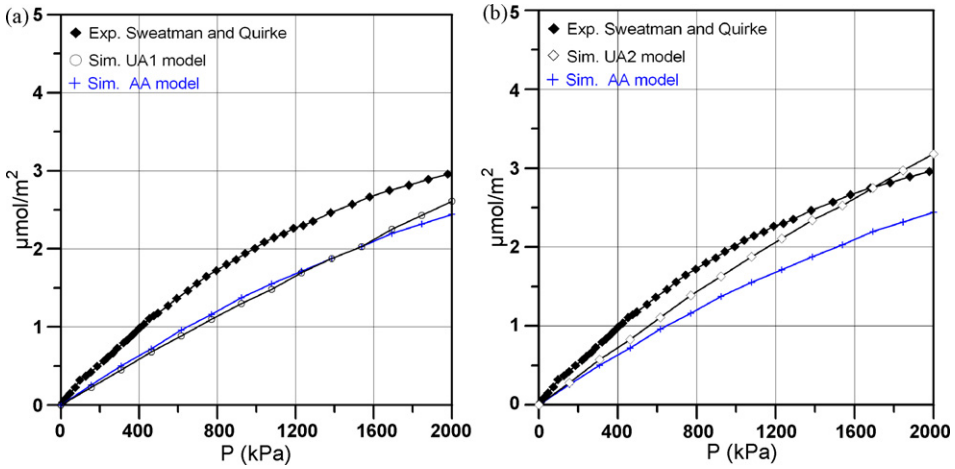

Fig. 2. Calculated adsorption isotherm of CH_4 at 298 K in slit carbon pore of H_{cc} = 70 Å. (a) AA model: crosses; UA1 model: circles; experimental: filled diamonds. (b) AA model: crosses; UA2 model: open diamonds; experimental: filled diamonds.

methane model. As expected, the AA model presents the largest pore in which adsorption was still possible (6.6 Å) while for the UA models adsorption was possible until a pore width of 6.4 Å. The excluded pore width H_e for adsorption of methane can be estimated as $H_e = H_{cc\,minimum} - \sigma_{ff}$. The equation that correlates the pore dimensions can be written as:

$$H_{eff} = H_{cc} - H_e$$

where H_{eff} is the effective internal pore size, H_{cc} is the carbon center-to-center pore size and H_e is the excluded pore width. The effective cell volume was calculated from the product of the surface area and the effective internal pore size (H_{eff}) as defined above.

The last step in deriving the pore size distribution from the measured collection of adsorption isotherm is by inverting the adsorption integral:

$$V(p) = \int_{H_{min}}^{H_{max}} f(H) v(H, p)\, dH$$

where $V(p)$ is the experimentally determined excess density, $f(H)$ is the required pore size distribution, and $v(H, p)$ is the excess volume at pressure p in a pore of size H. The integral is calculated over all pore sizes H.

Several methods for solving the above equation are known and have been used in previous studies, including best-fit methods and matrix methods. In this study, we used matrix methods where a system of linear equations is solved by matrix inversion with non-negativity constraints routine. Regularization was introduced based in the "L curve" criteria via a smoothing parameter [17,18]. This method is needed to stabilize the numerical computation, by incorporating additional constraints based on the smoothness of the PSD. The result can be stabilized avoiding that the fitting routine fits the data more closely than what is necessary from the conditioning of the system, which reduces the spikiness of the result, yielding more realistic PSDs [18].

3. Results and discussion

3.1. Adsorption isotherms on graphite surface

In Fig. 2, the simulated methane isotherms at 298 K calculated by GCMC for the AA and UA models in a wide slit pore of size H_{cc} = 70 Å are shown using surface excess (µmol/m^2) versus pressure (kPa). The experimental isotherms for Vulcan (a graphitic reference surface) from Sweatman and Quirke [5] are also shown.

As already explained (Section 2.1), to obtain the AA and UA1 unfitted models we left the AA model unchanged and modified the UA1 well depth parameter to fit the AA model. In Fig. 2a, we may observe the best fitting obtained between UA1 and AA models. The Vulcan experimental isotherm is also shown in Fig. 2a for comparison. Considering that the same conditions of solid–fluid parameterization were assured we shall then be able to compare unfitted AA and UA1 models in slit pores.

The fitted UA2 model uses the same Sweatman and Quirke [5] model as reference and was adjusted to match the experimental Vulcan isotherm. In spite of UA2 be our fitted model, it is clear that the experimental isotherms are more curved than the corresponding simulated isotherm and the fitting is rather poor (Fig. 2b). A similar result was obtained by Sweatman and Quirke [5] when they performed the fitting between the Vulcan experimental isotherm to their simulated UA model.

One of the most striking features of these results is that the AA model isotherm shape on the graphitic nonporous surface is much more similar to the experimental data than the UA model isotherms. While all UA isotherms are almost linear, the AA isotherm is curved. This is evidence that the AA model introduces some levels of heterogeneity to the system.

3.2. Adsorption isotherms on slit pores

3.2.1. Dependence of the loading on the cutoff distance

The process of computation energies for nonbond interactions reveals a quadratic dependence on the number of atoms in the system. Therefore, it is common to neglect the nonbond interaction for widely separated pairs of atoms. To maintain accuracy of the calculation with the minimum time possible, we performed a study of the dependence of the loading on the cutoff distance using the UA1 model. This study was also important because one needs to know if molecular simulation in literature based on different cutoffs can be compared. We recognize that the exact dependence varies and should be calibrated for each system. We selected 3 pores representing each one the main characterizing groups of isotherms (see next section) and varied the cutoff from 12 to 20 Å. The results are shown in Fig. 3. For systems in supercritical condition like methane at 303 K, we observe that the nonbonded potential presents small variations with cutoff. The adsorbed concentration tends to be invariant after the cut off of 20 Å. For the pore of 7 Å and for the low pressures range of the other pores, the difference between the cutoff of 12 and 20 was insignificant.

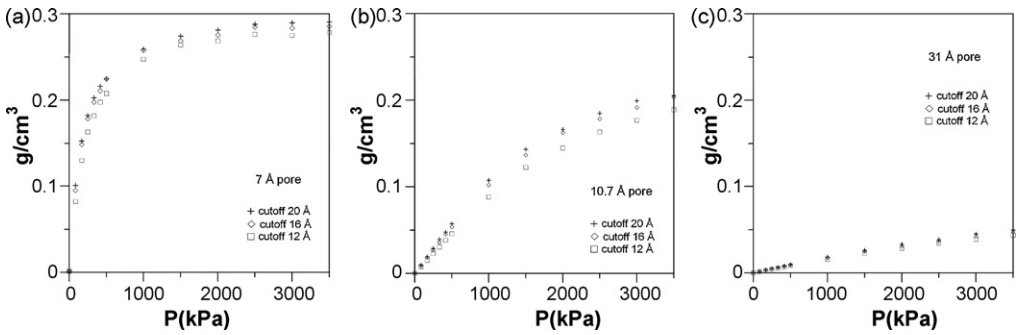

Fig. 3. Effect of the cutoff distance on the methane density at 302 K for UA1 model (a: 7 Å pore; b: 10.7 Å pore; c: 31 Å pore).

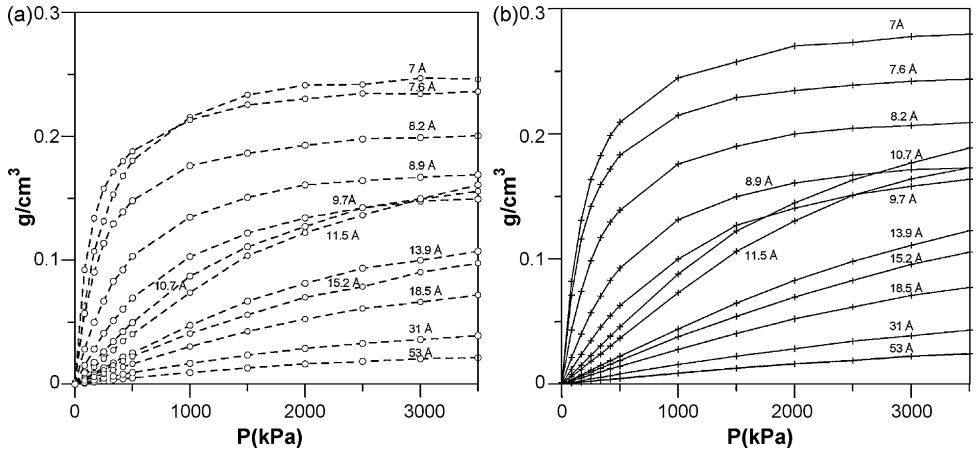

Fig. 4. Selected GCMC isotherms of methane at 303 K from AA (a) and UA1 (b) collections of 24 slit pores. The pores are expressed in H_{cc} (carbon center-to-center width). Points represent the individual simulated results. Lines between points are drawn only as a guide to the eye.

3.2.2. AA and UA1 kernels of simulated isotherms

For the AA and UA1 models, we calculated the local adsorption isotherm in the same set of 24 pores distributed logarithmically starting from the smallest pore in which adsorption was still possible until the maximum pore size of 53 Å. Using GCMC molecular simulations, the equilibrium isotherm of CH_4 was calculated at 303 K up to pressure of 3500 kPa. These pressure and temperature conditions are the same used to define the natural gas storage target by the U.S. Department of Energy. The excess adsorption isotherm for methane in models AA and AU1 are presented in Fig. 4.

All simulated isotherm are IUPAC type I. The three groups of behavior that was very useful for characterization using methane as probe-gas [3] can be observed in the collections of isotherms for the two models (AA and UA1). The first group includes isotherms of pores that can accommodate only one layer of molecules. In these pores, the adsorption occurs at low pressures and the isotherm becomes flat at relatively low pressures due to the strong confinement of the molecules in the pores. In this group, the maximum adsorption occurs at about 7 Å pore width. The second group includes isotherms that go approximately from 10 up to 18 Å. The pores of optimum dimensions for accommodating two layers of molecules are the main component of this group. When two layers are formed, the tendency of adsorption, that was decreasing as the pore dimensions increased, is reversed and causes a slight increase in adsorption at the high-pressure region. This can be observed clearly for the 11.5 Å pore that adsorbs more than the 9.7 Å pore, despite having lower wall potential. In the third group, we notice the isotherms for which the behavior is practically the same as the largest simulated pore (53 Å). In this pore range, the wall potential no longer overlaps and the cooperative effect of fluid–fluid interaction is rather small.

In spite of the models presenting the typical groups of isotherms well characterized, some outstanding differences occur between them. In the first group of isotherms (one layer group), the loading decreases much more intensely for the model UA1. This decrease is due to the smallest size of the UA1 model molecules. For this group of pores, where the wall potential is at a maximum, the UA1 model

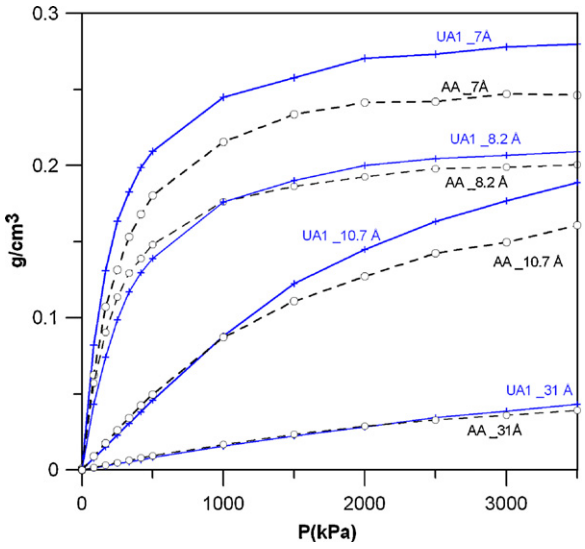

Fig. 5. GCMC isotherms of methane at 303 K from AA (circles) and UA1 (crosses) models for pore widths 7, 8.2, 10.7 and 31 Å. The pores are expressed in H_{cc} (carbon center-to-center width). Points represent the individual simulated results. Lines between points are drawn only as a guide to the eye.

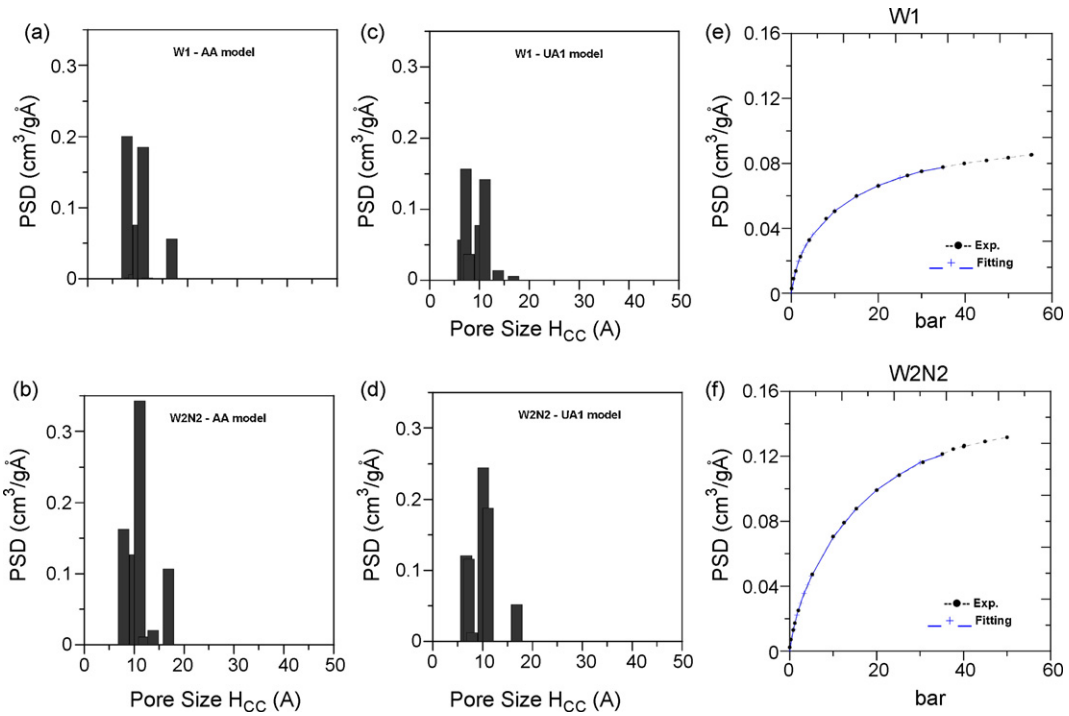

Fig. 6. Pore size distribution and isotherms for W1 and W2N2 samples. PSD calculated from AA and UA1 collection of methane isotherms at 303 K using GCMC (a–d). Theoretical fit obtained from the PSD of AA model of experimental isotherm. Experimental data: points; theoretical fit: line.

allows a better packing of pseudo-spherical particles than the 5-site AA model. Then, when the wall potential starts to decrease, the loading comes down in a more abrupt way. Another difference is that in the AA model adsorption at low pressures shows even higher values than in the UA1 model. This behavior can be explained by the largest adsorption heat presented by the AA model that is on average 7% larger than the value for the UA1 model, at this range of pore sizes.

Another notable difference between the two collections of isotherms is seen in the range of the second group (two layers pores). While in the AA model the 10.7 Å pore loading occurs in a smooth way, in the UA1 model it is more abrupt. Again

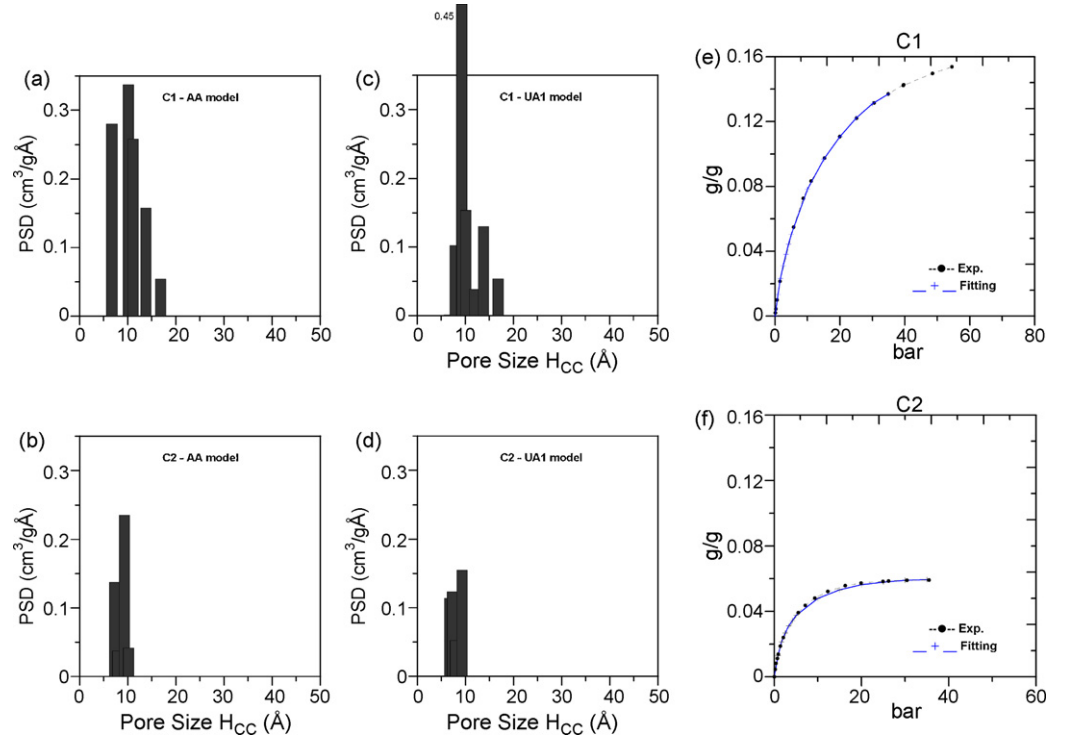

Fig. 7. Pore size distribution and isotherms for C1 and C2 samples. PSD calculated from AA and UA1 collection of methane isotherms at 303 K using GCMC (a–d). Theoretical fit obtained from the PSD of AA model of experimental isotherm. Experimental data: points; theoretical fit: line.

this behavior may be explained by the better packing of pseudo-spherical particles in a confined space maximizing the fluid–fluid interaction.

In Fig. 5 we compare typical isotherms for each of the characterizing behavior groups for the two models of methane molecule, so we can clearly notice the differences discussed previously. It may be observed that the UA1 model presents higher loadings when the confined space is at the optimum value for one adsorbed methane layer (7 Å) and for two adsorbed methane layers (10.7 Å). For the other pore sizes, such as 8.2 or 31 Å, the adsorption behavior is essentially the same for both models. We can also observe that except for the 7 Å slit width, in all other pore sizes the AA model presents higher adsorption capacities at low pressures.

3.2.3. Pore size distribution analysis

Four activated carbon samples were used in this study (W1, W2N2, C1 and C2). The samples W1 and W2N2 were prepared in our laboratory by chemical activation with H_3PO_4 from coconut shells. After impregnation, the samples were carbonized at 450 °C for 2 h. Details about the preparation may be found in Rios et al. [19]. The W1 sample was impregnated with phosphoric acid solutions at concentrations of 44% (w/w). For the W2N2 sample the phosphoric acid solutions concentrations were increased to 53% (w/w) and additional previous treatment of the W2N2 precursor were performed with sulfuric acid with the pyrolysis process carried out under nitrogen flow. Both surface area and micropore volume were substantially increased for this sample. Other two commercial samples named C1 and C2, with high and low surface area, respectively, are also used for comparison. Methane adsorption experiments at 303 K were performed in a gravimetric equipment using a magnetic suspension balance (Rubotherm, Germany).

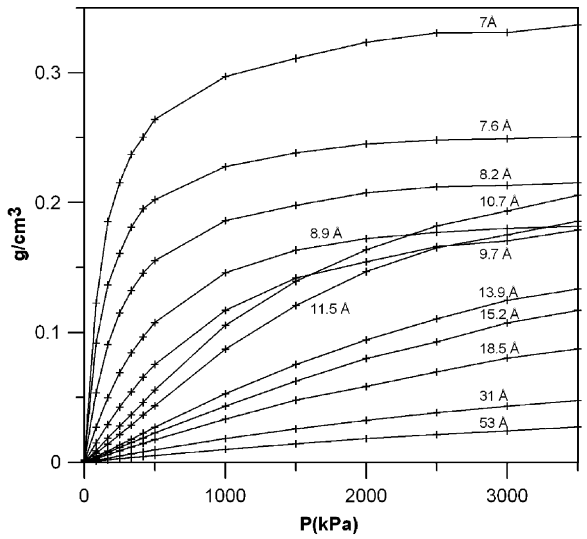

Fig. 8. Selected GCMC isotherms of methane at 303 K from UA2 collection of 24 slit pores. The pores are expressed in H_{cc} (carbon center-to-center width). Points represent the individual simulated results. Lines between points are drawn only as a guide to the eye.

All samples had been previously characterized using N_2 at 77 K [20]. Samples W2N2 and C1 have pores above 20 Å, thus outside the

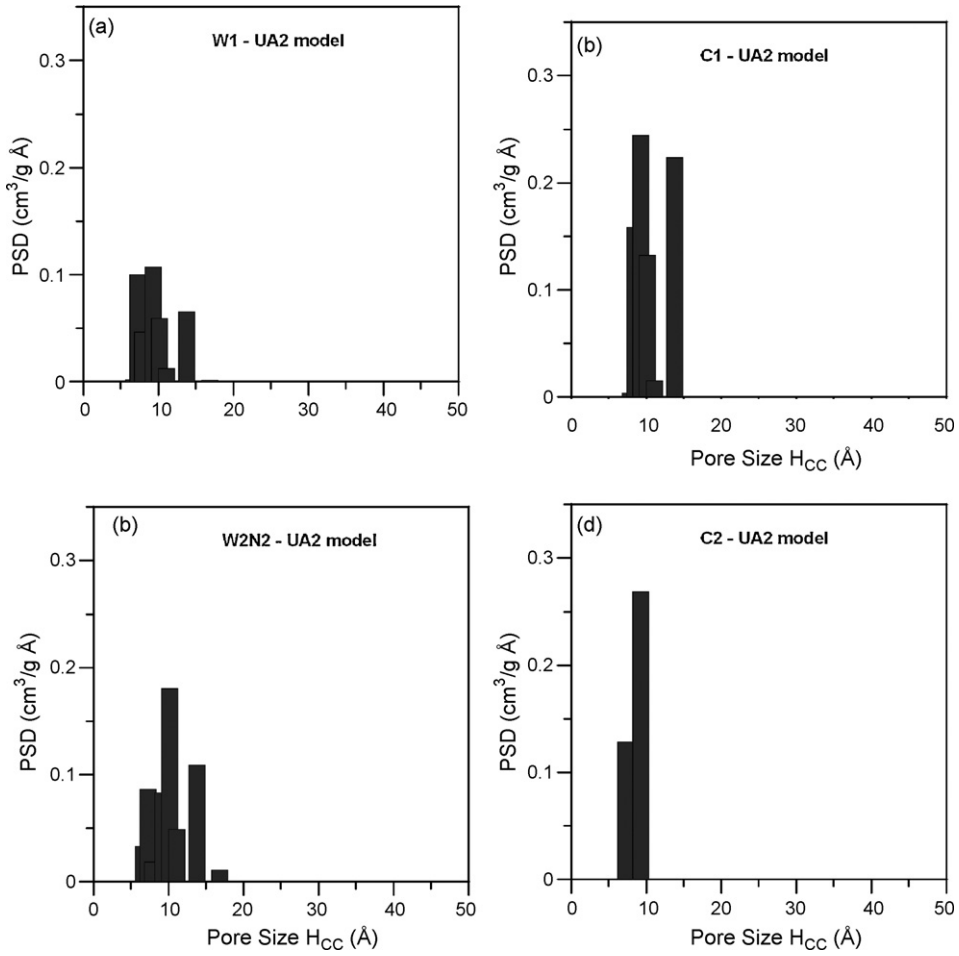

Fig. 9. (a–d) Pore size distribution of W1, W2N2, C1 and C2 active carbons calculated from UA2 collection of methane isotherms at 303 K using GCMC.

window of reliability estimated as 15.2 Å for models UA1 and UA2, and 18.5 Å for model AA (see supplementary material). It had been proposed by Gusev et al. [3] that the limiting accessible pore size for methane kernels is 20 Å. Therefore we decided to use only the simulated isotherms for pore sizes up to that limit for the determination of the PSDs in this study. As reported by Ravikovitch et al. [11], even when the carbon samples contain pores in sizes beyond the window of reliability, there is a very good agreement between PSDs calculated from the complete collection of isotherms and PSDs calculated from a collection of restricted pores sizes up to the limit of sensitivity of the constrained kernel.

Figs. 6 and 7 present the pore size distribution (PSD) calculated from the application of the isotherm collection of each model. The experimental and the theoretical fitted isotherms obtained from the PSD of the AA model are also shown. Only the AA model fitting results are plotted for the sake of clarity, since the UA1 model presented very similar results. Good fitting with the experimental isotherms were obtained with comparable low fitting errors for all analyzed samples. Analyzing first the samples W1 and W2N2 (Fig. 6) we expected that W2N2 would present a larger amount of micropores than W1 due to the higher degree of activation of W2N2 [21–23]. Both models were able to predict this trend.

The commercial sample C1 has higher surface area (2300 cm^2/g) than C2 (800 cm^2/g). Both models present PSD results compatible with this characteristic of the samples (Fig. 7) and also present good fitting with the experimental isotherms. The UA1 model tends to present pore volumes predominantly within the 10 Å range mainly for the C1 sample.

3.2.4. UA2 kernel and solid–fluid interaction impact in slit pores

To investigate the importance of the solid–fluid standard parameterization for this supercritical system we elaborated a new collection of isotherms (UA2) fitted to the Vulcan reference isotherm and then recalculated the PSD for the same samples W1, W2N2, C1 and C2. Selected isotherms for these pores are shown in Fig. 8. These isotherms are very similar to the UA1 isotherms. The only remarkable difference is the higher loading for the 7 Å isotherm (0.33 g/cm^3 at 3500 kPa) while for the UA1 model we had only 0.28 g/cm^3. The higher loading at 7 Å may be explained by the higher well depth (0.049 kcal mol^{-1}) of the UA2 model. For the next size of selected isotherm (7.6 Å) we had comparable loadings. For this pore size, the UA2 model adsorbs 0.25 g/cm^3 at 3500 kPa, while the UA1 model presented 0.24 g/cm^3. Even for the second layer pore of 10.7 Å the loadings are similar: 0.2 g/cm^3 and 0.19 g/cm^3 for UA2 and UA1 model, respectively.

Fig. 9 presents the pore size distribution calculated from the application of the isotherms collection using the UA2 model. Particularly for the C1 sample, differently from the unfitted UA1 model, the fitted UA2 model gives a PSD without any pore volume concentration. It was observed that the UA2 model presents PSDs more similar to the PSDs obtained using the unfitted AA model (see Figs. 6 and 7). The fitting between the simulated and experimental isotherms of the four activated carbon samples were as good as for the AA and UA1 models, with comparable low fitting errors.

4. Conclusion

The performance of all-atom (AA) and united atom (UA) models of the methane molecule were evaluated for the description of adsorption isotherms on a graphite surfaces and in a collection of slit pores. We performed GCMC calculations in explicit graphene model to elaborate three sets of isotherm collection for pseudo-spherical (UA models) and 5-point methane molecule model (AA model). These collections were used to calculate the pore size distribution (PSD) of four activated carbon samples. The influences of the cutoff and solid–fluid standard parameterization were also investigated.

In the graphite surface studies, we found that the simulated AA model isotherm shapes are much more similar to the experimental data than when the UA model isotherm was used. The UA model isotherms are linear while the AA isotherm is curved. This is an indication that a five-point methane model can induce heterogeneity effects in the slit-pore model.

Under the conditions of the analyzed supercritical system, the cutoff had little influence on the isotherms and the PSDs. Different solid–fluid standard parameterizations between UA1 and UA2 models modify the PSD.

The AA and UA models presented good theoretical fit with experimental isotherms, and the isotherm collections showed three main characterizing behavior groups (one layer, two layers and low wall potential). In the activated carbons that were studied, the UA1 model indicated less plausible PSD for C1 sample with pore size distributions predominantly around 10 Å. Our results suggest that both the AA and UA2 models yield more realistic estimates of the internal structure of microporous carbons.

Acknowledgements

The authors wish to acknowledge financial support for this study from CAPES, CNPq and FINEP/CTPETRO (Brazil) and CONICET (Argentina).

Appendix A. Supplementary data

Supplementary data associated with this article can be found, in the online version, at doi:10.1016/j.colsurfa.2009.12.015.

References

[1] N.A. Seaton, J.P.R.B. Walton, N. Quirke, A new analysis method for the determination of the pore size distribution of porous carbons from nitrogen adsorption measurements, Carbon 27 (1989) 853–861.
[2] C. Lastoskie, K.E. Gubbins, N. Quirke, Pore size distribution analysis of microporous carbons: a density functional theory approach, J. Phys. Chem. 97 (1993) 4786–4796.
[3] V.Y. Gusev, J.A. O'Brien, N.A. Seaton, A self-consistent method for characterization of activated carbons using supercritical adsorption and grand canonical Monte Carlo simulations, Langmuir 13 (1997) 2815–2821.
[4] N. Quirke, S.R.R. Tennison, The interpretation of pore size distributions of microporous carbons, Carbon 34 (1996) 1281–1286.
[5] M.B. Sweatman, N. Quirke, Characterization of porous materials by gas adsorption at ambient temperatures and high pressure, J. Phys. Chem. B 105 (2001) 1403–1411.
[6] M.V. Lopez-Ramon, J. Jagiello, T.J. Bandosz, N.A. Seaton, Determination of the pore size distribution and network connectivity in microporous solids by adsorption measurements and Monte Carlo simulation, Langmuir 13 (1997) 4435–4445.
[7] M.G. Martin, J.I. Siepmann, Transferable potentials for phase equilibria. 1. United-atom description of n-alkanes, J. Phys. Chem. B 102 (1998) 2569–2577.
[8] S. Murad, K.E. Gubbins, Computer modeling of matter, ACS Symp. Ser. 86 (1978) 62.
[9] S. Murad, D.J. Evans, K.E. Gubbins, W.B. Streett, D.J. Tildesley, Molecular dynamics simulation of dense fluid methane, Mol. Phys. 37 (1979) 725–736.
[10] H. Stassen, On the pair potential in dense fluid methane, J. Mol. Struct. (Theochem) 464 (1999) 107–119.
[11] P.I. Ravikovitch, A. Vishnyakov, R. Russo, A.V. Neimark, Unified approach to pore size characterization of microporous carbonaceous materials from N_2, Ar, and CO_2 adsorption isotherms, Langmuir 16 (2000) 2311–2320.
[12] W.A. Steele, The Interaction of Gases with Solid Surfaces, Pergamon, New York, 1974.
[13] K.T. Thomson, K.E. Gubbins, Modeling structural morphology of microporous carbons by reverse Monte Carlo, Langmuir 16 (2000) 5761–5773.
[14] D. Frenkel, B. Smit, Understanding Molecular Simulation, Academic Press, New York, 2002.
[15] G.M. Davies, N.A. Seaton, The effect of the choice of pore model on the characterization of the internal structure of microporous carbons using pore size distribution, Carbon 36 (1998) 1473–1490.
[16] Sorption, Invoked from Materials Studio v. 4.1, Accelrys Inc., San Diego, 2007.
[17] C.L. Lawson, R.J. Hanson, Solving Least Squares Problems, Siam, 1995.

[18] G.M. Davies, N.A. Seaton, Development and validation of pore structure models for adsorption in activated carbons, Langmuir 15 (1999) 6263–6276.
[19] R.B. Rios, F.W.M. Silva, A.E.B. Torres, D.C.S. Azevedo, C.L. Cavalcante Jr., Adsorption of methane in activated carbons obtained from coconut shells using H_3PO_4 chemical activation, Adsorption 15 (2009) 271–277.
[20] D.C.S. Azevedo, C.L. Cavalcante, R.H. López, A.E.B. Torres, J.P. Toso, G. Zgrablich, Mixed geometry characterization of activated carbons PSD, in: N. Seaton, F. Rodriguez-Reinoso, P. Llewellyn, S. Kaskell (Eds.), Characterisation of Porous Solids VIII – Proceedings of the 8th International Symposium on the Characterisation of Porous Solids, RSC Publishing, Cambridge, 2009, pp. 211–217.
[21] M. Molina-Sabio, F. Rodriguez-Reinoso, Role of chemical activation in the development of carbon porosity, Colloid Surf. A: Physicochem. Eng. Aspects 241 (2004) 15–25.
[22] M.V. Navarro, N.A. Seaton, A.M. Mastral, R. Murillo, Analysis of the evolution of the pore size distribution and the pore network connectivity of a porous carbon during activation, Carbon 44 (2006) 2281–2288.
[23] E.A. Ustinov, D.D. Do, V.B. Fenelonov, Modeling of heterogeneous surfaces and characterization of porous materials by extending density functional theory for the case of amorphous solids, Appl. Surf. Sci. 253 (2007) 5610–5615.